arXiv:0908.0933v1 [astro-ph.HE] 6 Aug 2009

# High-energy flares from jet-clump interactions

Anabella T. Araudo[1,2] Valentí Bosch-Ramon[3] and Gustavo E. Romero[1,2]

[1] *Instituto Argentino de Radioastronomía (CCT La Plata, CONICET), C.C.5, 1894 Villa Elisa, Buenos Aires, Argentina*
[2] *Facultad de Ciencias Astronómicas y Geofísicas, Universidad Nacional de La Plata, Argentina*
[3] *Max Planck Institut für Kernphysik, Saupfercheckweg 1, Heidelberg 69117, Germany*

**Abstract.** High-mass microquasars are binary systems composed by a massive star and a compact object from which relativistic jets are launched. Regarding the companion star, observational evidence supports the idea that winds of hot stars are formed by clumps. Then, these inhomogeneities may interact with the jets producing a flaring activity. In the present contribution we study the interaction between a jet and a clump of the stellar wind in a high-mass microquasar. This interaction produces a shock in the jet, where particles may be accelerated up to relativistic energies. We calculate the spectral energy distributions of the dominant non-thermal processes: synchrotron radiation, inverse Compton scattering, and proton-proton collisions. Significant levels of X- and $\gamma$-ray emission are predicted, with luminosities in the different domains up to $\sim 10^{34} - 10^{35}$ erg s$^{-1}$ on a timescale of about $\sim 1$ h. Finally, jet-clump interactions in high-mass microquasars could be detectable at high energies. These phenomena may be behind the fast TeV variability found in some high-mass X-ray binary systems, such as Cygnus X-1, LS 5039 and LS I+61 303. In addition, our model can help to derive information on the properties of jets and clumpy winds.

## 1. Introduction

The mass loss in massive stars is thought to take place via supersonic inhomogeneous winds. Considerable observational evidence supports the idea that the wind structure is clumpy (e.g. Owocki & Cohen 2006), although the properties of clumps are not well-known as a cosequense of the high spatial resolution necessary for the clumps detection. Some massive stars are accompanied by a compact object and present transfer of matter to it forming an accretion disk and, in high-mass microquasars (HMMQs), bipolar relativistic outflows.

Non-thermal emission has been observed in microquasar jets from radio to X-rays, and it is thought that $\gamma$-rays could be also produced in jets. Recently, a TeV flare has been detected from the HMMQ Cygnus X-1 (Albert et al. 2007). Transient $\gamma$-ray events could have been detected as well from the high-mass X-ray binaries LS 5039 (Aharonian et al. 2005), LS I+61 303 (Albert et al. 2006) and perhaps from the HMMQ Cygnus X-3 (ATels 1492, 1547 and 1585). Some authors have been suggested that this strongly variable $\gamma$-ray emission

can be produced by the interaction between the jet and the stellar wind of the companion star (e.g. Owocki et al. 2009, Araudo et al. 2009).

In the present contribution we propose a model to explain these $\gamma$-ray flares based on the interaction between the jets of a HMMQ with wind inhomogeneities. The clumps can eventually penetrate in the jet, leading to transient non-thermal activity that may release a significant fraction of the jet kinetic luminosity in the form of synchrotron, inverse Compton (IC), and proton-proton ($pp$) emission.

## 2. The scenario

To study the interaction between a clump of the stellar wind and a jet in a HMMQ, we adopt a scenario with similar characteristics to Cygnus X-1. We fix the separation between the compact object and the massive star to $a = 3 \times 10^{12}$ cm. The stellar mass loss rate is adopted to be $\dot{M}_\star = 3 \times 10^{-6}\, M_\odot\, \mathrm{yr}^{-1}$, with a terminal wind velocity $v_\mathrm{w} \sim 2.5 \times 10^8\ \mathrm{cm\ s}^{-1}$. A sketch of the scenario is presented in Figure 1.

### 2.1. Clump and jet model

The clump is taken to be spherical and we consider two values of it radius: $R_\mathrm{c} = 10^{10}$ and $10^{11}$ cm. We have assumed that the velocity of the clumps is equal to the velocity of the wind, i.e $v_\mathrm{c} = v_\mathrm{w}$. In order to obtain a large density contrast between the clump and the jet we assume dense and homogeneous clumps with $n_\mathrm{c} = 10^{12}\ \mathrm{cm}^{-3}$, which corresponds to a clumpy wind filling factor of $f = \dot{M}_\star/4\pi a^2 m_p v_\mathrm{c} n_\mathrm{c} = 0.005$, where $m_p$ is the mass of the proton.

We consider a jet dynamically dominated by cold protons with a bulk velocity $v_\mathrm{j} = 0.3\,c$ and a kinetic luminosity $L_\mathrm{kin} \sim 3 \times 10^{36}\ \mathrm{erg\ s}^{-1}$ (e.g. Gallo et al. 2005). We assume here that the jet radius is one tenth of the jet height, i.e. $R_\mathrm{j}(z) = 0.1\,z$, and the jet-clump interaction is taken to occur at $z_\mathrm{int} = a/2$. The density of the jet material at $z_\mathrm{int}$ results $n_\mathrm{j} = 4.7 \times 10^7\ \mathrm{cm}^{-3}$ and then, the ratio between the clump and the jet densities is $\chi = 2.1 \times 10^4$. This parameter will be very relevant for the jet-clump interaction estimates.

### 2.2. Dynamics of the interaction

In order to study the physical processes of the jet-clump interaction, we consider the collision of a single clump with the jet. The huge density contrast $\chi$ allows the clump to cross the boundary of the jet and fully penetrate into it. In the context of this work, thermal conduction, clump expansion, magnetic fields and gravitational forces are not dynamically relevant for the jet-clump interaction and will be neglected.

In the Laboratory Reference Frame (LRF), the clump will take a time $t_\mathrm{c}$ to fully enter the jet and a time $t_\mathrm{j}$ to cross it roughly at the wind velocity:

$$t_\mathrm{c} \sim 2\,R_\mathrm{c}/v_\mathrm{c} \sim 80 \text{ s } (\mathrm{R_c} = 10^{10} \text{ cm}) \text{ and } \sim 800 \text{ s } (\mathrm{R_c} = 10^{11} \text{ cm}), \qquad (1)$$

$$t_\mathrm{j} \sim \frac{2\,R_\mathrm{j}}{v_\mathrm{c}} = 1.2 \times 10^3 \text{ s.} \qquad (2)$$

When the clump interacts with the jet, a shock is formed in the clump and propagates in the direction of the jet motion with a velocity $v_{cs} \sim v_j/\sqrt{\chi}$. The clump-crossing time, which is the characteristic timescale of the jet-clump interaction, can be defined as:

$$t_{cc} \sim \frac{2\,R_c}{v_{cs}} \sim 3 \times 10^2 \text{ s } (R_c = 10^{10} \text{ cm}) \text{ and } \sim 3 \times 10^3 \text{ s } (R_c = 10^{11} \text{ cm}). \quad (3)$$

A shock (the bow shock) is also formed in the jet when its material collides with the clump. We assume the clump/bow-shock separation distance as $x \sim 0.2R_c$ (van Dyke & Gordon 1959), and thus the time required to reach the steady state regime results:

$$t_{bs} \sim \frac{0.2R_c}{v_{j\ ps}} \sim \frac{0.2R_c}{v_j/4} \sim \frac{5}{2}\frac{t_{cc}}{\sqrt{\chi}} \ll t_{cc}. \quad (4)$$

Once the clump is inside the jet, the latter accelerates the clump up to the background velocity, $v_j$, with an acceleration $g \sim v_j^2/\chi R_c$ (e.g. Fragile et al. 2004) in a time

$$t_g \sim \frac{v_j}{g} \sim \sqrt{\chi}\,t_{cc} \gg t_{cc}. \quad (5)$$

When one fluid exerts a force against another fluid of different density, the hydrodynamical Rayleigh-Taylor (RT) instability eventually develops, leading to the perturbation and potential disruption of the clump. On the other hand, after the bow shock is formed, the jet material surrounds the clump and we have two fluids with a large relative velocity (in our case $\sim v_j$). This situation leads to Kelvin-Helmholtz (KH) instabilities. The timescale for these instabilities, considering that the length of the perturbed region is $\sim R_c$, are:

$$t_{RT} \sim \sqrt{R_c/g} \sim t_{cc} \quad \text{and} \quad t_{KH} \sim \frac{R_c\,\sqrt{\chi}}{v_j} \sim t_{cc}. \quad (6)$$

We assume that for a $t_c \sim t_{cc}/5$ we can treat the jet-clump interaction as the clump were fully inside the jet. At this stage we do not consider the penetration of the clump into the jet, and assume in our treatment that the former is completely inside the latter (i.e. the system has cylindrical symmetry; see Fig. 1). We notice that the clump might not escape the jet if $t_j > t_{RT/KH}$ due to disruption through instabilities, although numerical simulations show that the instability timescales are actually longer than the clump crossing time by a factor of a few ( e.g. Klein, McKee & Colella 1994).

## 3. Non-thermal processes

Given the characteristics of our scenario, the shock in the clump is radiative, and the bow shock is adiabatic. For these reasons, the shocked and heated material of the clump will radiate (by thermal Bremsstrahlung) a non-negligible part of the energy tranferred by the jet, whereas in the bow shock non-thermal processes take place. We focus here in the non-thermal emission.
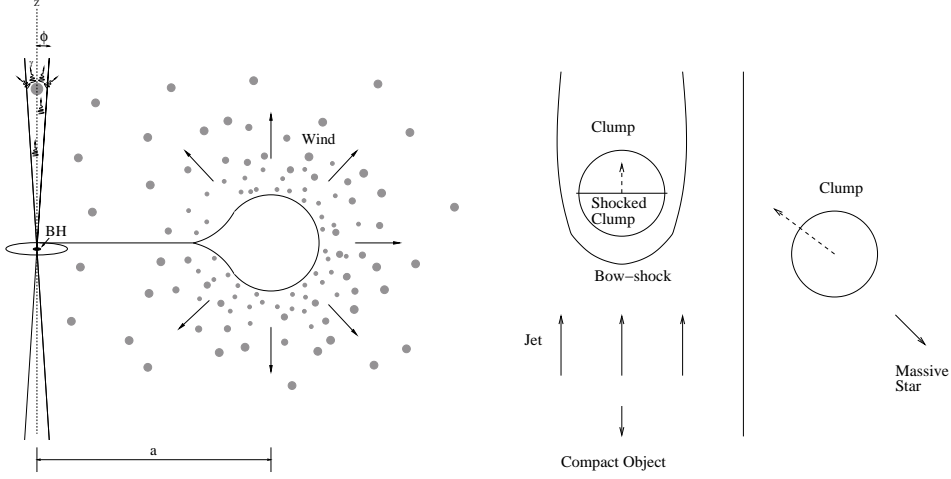
Figure 1.     Sketch of a HMMQ with a clumpy wind (left) and the jet-clump interaction (right).

## 3.1.    Particle acceleration and radiative cooling

Assuming that non-relativistic diffusive (Fermi I) shock acceleration takes place in the bow-shock, electrons and protons with a charge $q$ will be accelerated up to an energy $E_{e,p}$ in a time

$$t_{\rm acc} = \frac{8}{3} \left( \frac{c}{v_{\rm j}} \right)^2 \frac{E_{e,p}}{q\,B_{\rm bs}\,c}\,, \qquad (7)$$

in the Bohm limit and for perpendicular shocks (Protheroe 1999). The magnetic field in the acceleration region is $B_{\rm bs}$, and we will consider two values for it. First, we consider a value obtained assuming that the magnetic energy density is a $10\,\%$ of the plasma internal energy density downstream and we obtain $B_{\rm bs} = 150$ G. We adopt a sub-equipartition value to make $B_{\rm bs}$ dynamically negligible with respect to matter. In addition, we adopt $B_{\rm bs} = 1$ G to check the impact on our results of a magnetic field much smaller than in the sub-equipartition case.

In the scenario presented in this work, relativistic leptons lose their energy mainly by synchrotron radiation and IC scattering. The former have the following cooling time

$$t_{\rm syn} = \frac{4.1 \times 10^2}{B_{\rm bs}^2\,E_e}\ {\rm s}\,. \qquad (8)$$

At $z_{\rm int}$, the energy density of the photons from the star is $u_{\rm ph} = 2.4 \times 10^2$ erg cm$^{-3}$, being the typical photon energy $\epsilon_0 \sim 10$ eV. For $y = \epsilon_0 E_e/(5.1 \times 10^5\,{\rm eV})^2 > 1$ the IC interaction takes place in the Klein-Nishina (KN) regime. A formula for the IC cooling time valid in both Thompson (Th) and KN regime under a photon field with a narrow energy distribution is (e.g. Bosch-Ramon & Khangulyan 2009):

$$t_{\rm IC} = \frac{6.1 \times 10^{12}\,\epsilon_0}{u_{\rm ph}}\,\frac{(1+8.3y)}{\ln(1+0.2\,y)}\,\frac{(1+1.3y^2)}{(1+0.5y+1.3y^2)}\ {\rm s}\,. \qquad (9)$$

Regarding hadronic emission, $\gamma$-rays are produced if relativistic protons interact with nuclei through inelastic $pp$ collisions, beeing the proton cooling time

$$t_{pp} = \frac{2.2 \times 10^{15}}{4n_{\rm j} \left(0.95 + 0.06\ln\left(\frac{E_p}{1.1m_p c^2}\right)\right)} \text{ s.} \tag{10}$$

In the bow-shock region, this process is negligible. Otherwise, if relativistic protons accelerated in the bow shock penetrate into the clump, $pp$ interactions can become an efficient process to generate $\gamma$-rays because $n_{\rm c} \gg n_{\rm j}$.

Besides radiative cooling, the escape of particles from the acceleration region is another kind of energy losses. The corresponding timescale, $\tau_{\rm esc}$, takes into account the advection of relativistic particles by downstream bow-shock material ($t_{\rm adv} \sim R_{\rm c}/v_{\rm j\,ps}$) and the diffusion of particles ($t_{\rm diff} \sim x^2/2D_{\rm B}$, where $D_{\rm B}$ is the Bohm diffusion coefficient), being $\tau_{\rm esc} = \min\{t_{\rm diff}, t_{\rm adv}\}$. Equating energy gains and losses, the maximum energy achieved by electrons ($E_e^{\rm max}$) accelerated in the bow shock is estimated (see Fig. 2). On the other hand, the maximum energy for protons ($E_p^{\rm max}$) is constrained by the size of the acceleration region. In Table 1, $E_e^{\rm max}$ and $E_p^{\rm max}$ are shown.


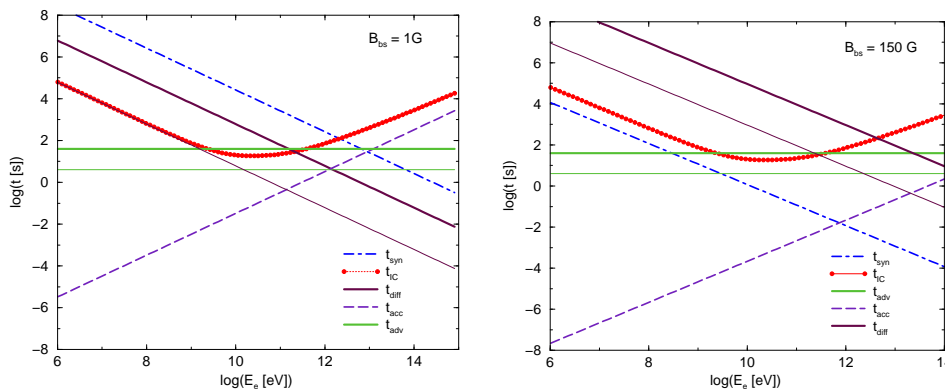
Figure 2. Acceleration and radiative loss time for electrons in the bow-shock region. The advection and diffusion times are shown for $R_{\rm c} = 10^{10}$ (thin line) and $10^{11}$ cm (thick line).

Table 1. Maximum energies achieved by acelerated particles in the bow shock and the energy break of electrons.

| $R_{\rm c}$ [cm] | $10^{10}$ | $10^{10}$ | $10^{11}$ | $10^{11}$ |
|---|---|---|---|---|
| $B_{\rm bs}$ [G] | 1 | 150 | 1 | 150 |
| $E_e^{\rm max}$ [eV] | $1.5 \times 10^{11}$ | $8 \times 10^{11}$ | $1.5 \times 10^{12}$ | $8 \times 10^{11}$ |
| $E_p^{\rm max}$ [eV] | $6 \times 10^{11}$ | $9 \times 10^{13}$ | $6 \times 10^{12}$ | $9 \times 10^{14}$ |
| $E_{\rm b}$ [eV] | $4.5 \times 10^{10}$ | $3 \times 10^{9}$ | $4.5 \times 10^{11}$ | $3 \times 10^{8}$ |

## 3.2.　High energy emission

In this section we calculate the Spectral Energy Distribution (SED) of the emission produced by the most relevant non-thermal radiative processes: synchrotron and IC radiation in the bow-shock region and $pp$ in the clump.

　　We assume an injected population of relativistic particles in the bow-shock region that follows a power-law energy distribution of the form:

$$Q_{e,p}(E_{e,p}) = K_{e,p}\, E_{e,p}^{-2}\, \exp(-E_{e,p}/E_{e,p}^{\mathrm{max}}) \,, \qquad (11)$$

typical for Fermi I acceleration. The normalization constant $K_{e,p}$ is determined assuming that the (non-thermal) luminosity of accelerated particles is $L_{\mathrm{NT}} = 0.25(R_{\mathrm{c}}/R_{\mathrm{j}})^2 L_{\mathrm{kin}}$ (note that the predicted fluxes scale linearly with the adopted non-thermal fraction 0.25). To estimate the particle energy distribution $N_{e,p}$, we solve the kinetic equation in the one-zone model approximation for the bow-shock region (e.g. Ginzburg & Syrovatskii 1964):

$$\frac{\partial N_{e,p}}{\partial t} + \frac{\partial}{\partial E_{e,p}}\Big(\frac{dE_{e,p}}{dt} N_{e,p}\Big) + \frac{N_{e,p}}{\tau_{\mathrm{esc}}} = Q_{e,p} \,. \qquad (12)$$

　　The relativistic leptons reach the steady state well before the shock has crossed the clump. Particles downstream with low energies escape advected in the shocked material of the jet before cooling radiatively, producing a break in the energy spectrum of particles. From $t_{\mathrm{adv}} = t_{\mathrm{syn}}$ and $t_{\mathrm{adv}} = t_{\mathrm{diff}}$ we determine the electron break energies $E_{\mathrm{b}}$. The values are shown in Table 1. The most energetic electrons can diffuse up to the clump ($B_{\mathrm{bs}} = 1$ G) or lose their energy inside the bow-shock region by synchrotron and IC radiation ($B_{\mathrm{bs}} = 150$ G). We note that the electrons with energies $E_e > E_{\mathrm{b}}$ can reach the clump and radiate inside it. In this work, we do not estimate the lepton emission in the clump.

　　As noted in Sect. 3.1., relativistic protons do not suffer significant $pp$ losses in the bow-shock region ($t_{\mathrm{diff}} \ll t_{pp}$). These protons can also reach the clump if they are not advected by the shocked material of the jet. Imposing that $t_{\mathrm{diff}} < t_{\mathrm{adv}}$, the minimum energy necessary to reach the clump is $E_p^{\mathrm{min}} = 0.025 E_p^{\mathrm{max}}$, and the maximum energies of these protons are shown in Table 1. On the other hand, to confine relativistic protons in the clump requires a very large magnetic field and we assume that protons will cross the whole clump in a time $\sim R_{\mathrm{c}}/c < t_{pp}$. Then, the distribution of relativistic protons in the clump is $N_p(E_p) = (R_{\mathrm{c}}/c) Q_p(E_p)$.

　　With the steady distributions of relativistic electrons in the bow shock, $N_e(E_e)$, and protons in the clump, $N_p(E_p)$, we calculate the SEDs. We estimate the specific luminosity as

$$\epsilon L(\epsilon) = \epsilon \int_{E_{e,p}^{\mathrm{min}}}^{E_{e,p}^{\mathrm{max}}} N_{e,p}(E_{e,p})\, j(E_{e,p}, \epsilon)\, dE_{e,p} \,, \qquad (13)$$

where $j(E_e, \epsilon)$ is the emissivity of the process and $\epsilon$ is the photon energy.

　　Synchrotron and IC emissivities are computed using the standard formulae given in Blumenthal & Gould (1970). For the later process we consider the parametrized differential cross section valid in both Th and KN regimes and $\pi^0$-decay emissivity is calculated following Kelner et al. (2006). The synchrotron

emission is computed in the optically thin case, neglecting the impact of synchrotron self-absorption, but at high energies (IC and *pp*) $\gamma - \gamma$ absorption is taken into account.

Synchrotron emission is dominant at X-rays for $B_{\mathrm{bs}} = 150$ G, with $L_{\mathrm{syn}} \sim 10^{35}$ erg s$^{-1}$. Inverse Compton scattering produces $\gamma$-rays up to very high energies, dominating the radiation output in the cases with $B_{\mathrm{bs}} = 1$ G. In our calculations, the highest luminosity achieved is $L_{\mathrm{IC}} \sim 10^{35}$ erg s$^{-1}$ for $R_{\mathrm{c}} = 10^{11}$ cm, although $\gamma - \gamma$ absorption can reduce substantially the emission above 100 GeV. Proton-proton collisions in the clump can also produce $\gamma$-rays at energies that may be as high as $\sim 10^{14}$ eV ($B_{\mathrm{bs}} = 150$ G). The maximum luminosity obtained by *pp* is nevertheless quite modest, $L_{pp} \sim 10^{32}$ erg s$^{-1}$ for $R_{\mathrm{c}} = 10^{11}$ cm, although denser and/or bigger clumps, and more powerful jets may yield detectable amounts of photons outside the $\gamma - \gamma$ absorption range (0.1-10 TeV). The computed SEDs are shown in Fig. 3, only for the cases with $B_{\mathrm{bs}} = 150$ G.
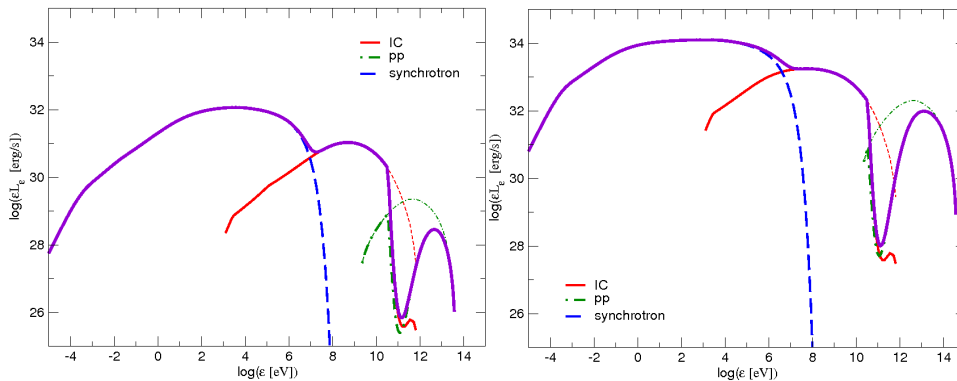


Figure 3.    Leptonic and hadronic emission from the bow shock and from the clump, respectively, for $B_{\mathrm{bs}} = 150$ G, and $R_{\mathrm{c}} = 10^{10}$ (left) and $10^{11}$ cm (right). The curves of both absorbed (thick lines) and unabsorbed (thin lines) IC and *pp* radiation are shown.

## 4.    Effect of many clumps

In general, many clumps can interact with the jet and is possible to have several clumps inside it simultaneously (see Owocki et al. 2009). However, at $z < z_{\mathrm{c}} = 4 \times 10^{11}$ cm the destruction time $t_{\mathrm{cc}}$ is less than the penetration one ($t_{\mathrm{c}}$) and the clump will be destroyed before completely entering into the jet. Then, the model presented here is not valid at $z < z_{\mathrm{c}}$ (neither if $R_{\mathrm{j}} < R_{\mathrm{c}}$).

Considering a canonical geometry for the jet and a filling factor of the wind $f = 0.005$, we estimate the number of clumps -$N_{\mathrm{c}}$- inside the jet, from $z = z_{\mathrm{c}}$ up to $z \sim a$. We obtain $N_{\mathrm{c}} \sim 350$ and $\sim 0.5$ for $R_{\mathrm{c}} = 10^{10}$ and $10^{11}$ cm, respectively. As a consecuence, flares produced by jet-clump interactions could be a sporadic phenomenon, for a low $N_{\mathrm{c}}$ ($R_{\mathrm{c}} = 10^{11}$ cm), or may appear as a modulated steady activity, for a high $N_{\mathrm{c}}$ ($R_{\mathrm{c}} = 10^{10}$ cm). In the latter case, the resulting SED will be similar than the obtained in the previous section, but

multiplied by $N_c$. Nevertheless, we note that the jet may be disrupted in those cases when too many clumps are simultaneously present inside the jet (Araudo et al. 2009). However, more detailed calculations of the dynamics of the jet-clump interaction are required to clarify this issue.

## 5.   Conclusions

In the present work, we study the main physical processes and the radiative outcomes from the interaction between the jet of a HMMQ with a clump of the companion stellar wind. This interaction produces a bow-shock in the jet where particles are accelerated up to very-high energies. The relativistic electrons are cooled efficiently by synchrotron and IC radiation in the bow shock, and protons by $\pi^0$-decay from $pp$ interactions in the clump.

Due to characteristics of the interaction, the expected emission can be transient if $N_c$ is low. Given the typical dynamical timescales, the flare duration may last from minutes to a few hours. The flares of jet-clump interactions would have associated lower (synchrotron) and higher energy components (IC, $pp$ emission). The total level of emission, the importance of the different components, and the duration of the flares, can give information on the jet power and size, clump size and density, and magnetic fields in the interaction regions. Therefore, besides the jet itself, the clump properties can be probed by observations at high energies of transient activity in HMMQs, being a new tool to study the winds of massive stars.

**References**

Aharonian, F. A., et al., 2005, Science, 309, 746
Albert, J., et al. 2006, Science, 312, 1771
Albert, J., et al., 2007, ApJ, 665, L51
Araudo, A. T,, Bosch-Ramon, V. & Romero G. E., 2009, A&A, submitted
Blumenthal, G.R., Gould, R.J., 1970, Rev. Mod. Phys., 42, 237
Bosch-Ramon, V. & Khangulyan, D., 2009, International Journal of Modern Physics D, in press [arXiv:0805.4123]
Fragile, P.C., Murray, S.D., Anninos, P. & van Breugel, W., 2004, ApJ, 604, 74
Ginzburg, V.L., Syrovatskii, S.I., 1964, The Origin of Cosmic Rays, Pergamon Press, New York
Kelner, S.R., Aharonian, F.A., & Vugayov, V.V., 2006, Phys. Rev. D, 74, 034018
Klein, R.I., McKee, C.F. & Colella, P., 1994, ApJ, 420, 213
Owocki, S. P., & Cohen D. H., 2006, ApJ, 648, 5650
Owocki, S.P., Romero G.E., Townsend, R. & Araudo, A.T., 2009, ApJ, 696, 6900
Protheroe, R.J., 1999, in: *Topics in cosmic-ray astrophysics*, eds. M. A. DuVernois (Nova Science Publishing), p. 240
van Dike & Gordon, H., 1959, NASA TR R-1